Electronic Supplementary Material (ESI) for Journal of Materials Chemistry A.

Supplementary information for

Li_2S/Carbon Nanocomposite Strips from a Low-Temperature Conversion of Li_2SO_4 as High-Performance Lithium-Sulfur Cathodes

Fangmin Ye, Hyungjun Noh, Jinhong Lee, Hongkyung Lee, and Hee-Tak Kim *

Table S1. Comparison of the Li_2S electrodes derived from the conversion of Li_2SO_4。

Cathode	Conversion Temperature (°C)	Electrode Preparation and Li_2S content in the cathode electrode	Potential window for initial cycle	Initial discharge capacity	Cycle capacity (mAh/g)	Ref.
Li_2S@C	900	Al-current collector 49.6 wt.%	1.5~3 V	0.5 C, 330	280 after 40 at 0.5 C	1
Li_2S-C	820	Al-current collector 68 wt.%	1.8~3.4 V	0.1 C, 700	450 after 50 at 0.1 C	2
Li_2S-GANs	900	Al-current collector 37.3%	1.6~4 V	0.05 C 620	320 after 50 at 0.2 C	3
Li_2S-rGO	900	Al-current collector 36 wt.%	1.5~4 V	0.025 C 950	469 after 100 at 0.1 C	4
Li_2S-KB	780	Al-current collector 60 wt%	1.5~4.4 V	1/12 C 693	508 after 40 at 1/12 C	5
Li_2S@C-CP	820	No-current collector 36 wt.%	1.7~3.8 V	0.1 C 820	430 after 100 at 0.1 C	6
Li_2S@C-CNT	635	No-current collector 40 wt.%	1.9~3.2 V	0.1 C, 805	595 after 150 at 0.2 C	This work

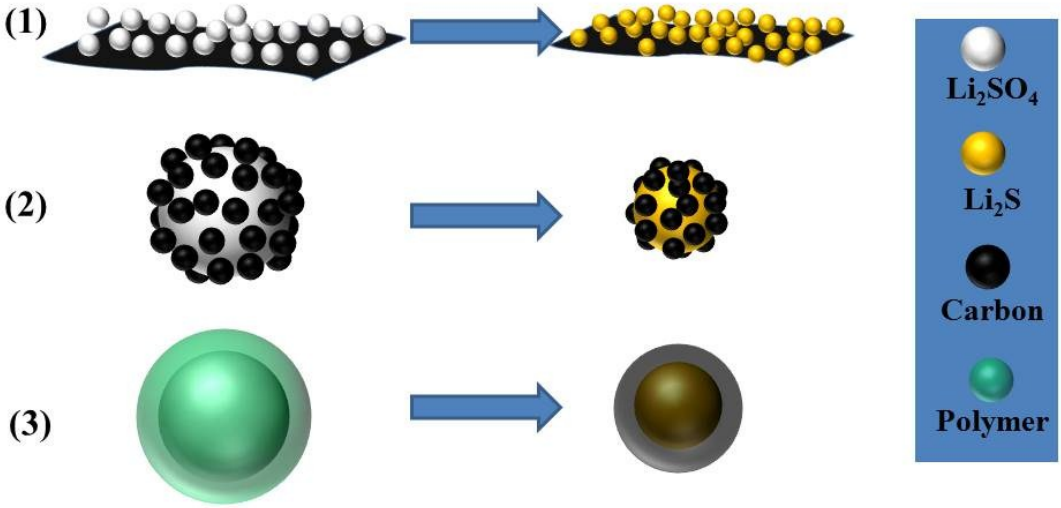

Figure S1. Schematic for three routes to fabricate carbon-coated Li_2S from Li_2SO_4. (1) Reduced graphene oxide (rGO) loaded Li_2SO_4 to prepare the rGO-Li_2S composite, (2) carbon particles coated Li_2SO_4 to prepare the Li_2S-C composite, (3) polymer coated Li_2SO_4 to prepare the Li_2S-C composite.

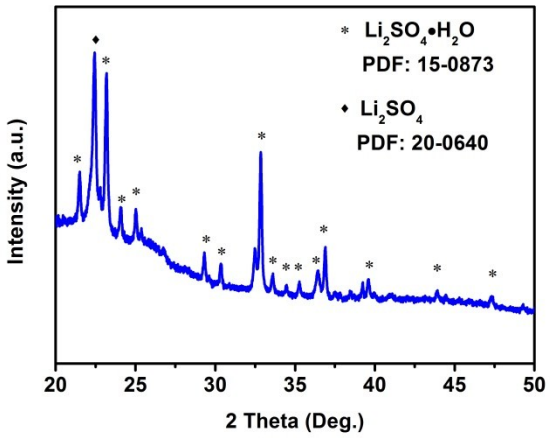

Figure S2. XRD pattern for the as-prepared Li_2SO_4@PVA-CNT nanocomposites.

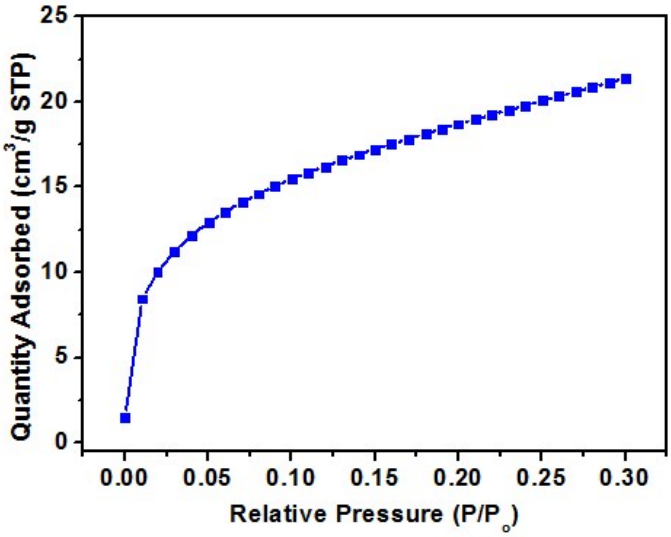

Figure S3. The isotherm adsorption curve for the as-prepared Li_2SO_4@PVA-CNT electrode.

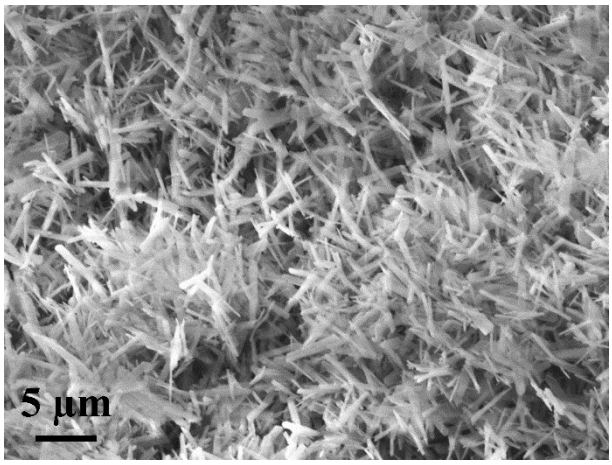

Figure S4. A low magnified SEM image of the as-prepared pure Li_2SO_4 microstrips without PVA and CNT prepared by adding the PVA-free Li_2SO_4 aqueous solution into icy ethanol.

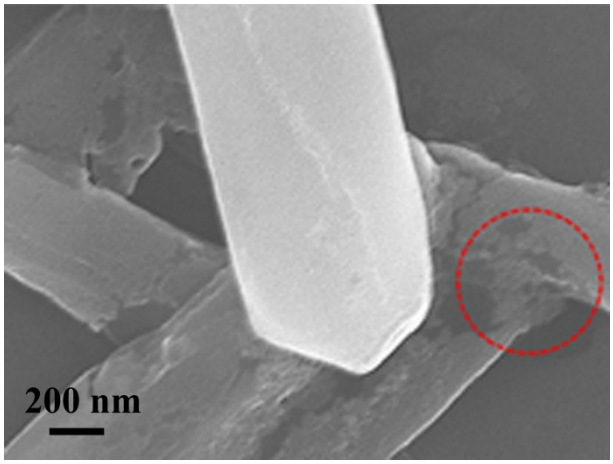

Figure S5. A high magnified SEM image of the pure Li_2SO_4 microstrips without PVA and CNT prepared by adding the PVA-free Li_2SO_4 aqueous solution into icy ethanol.

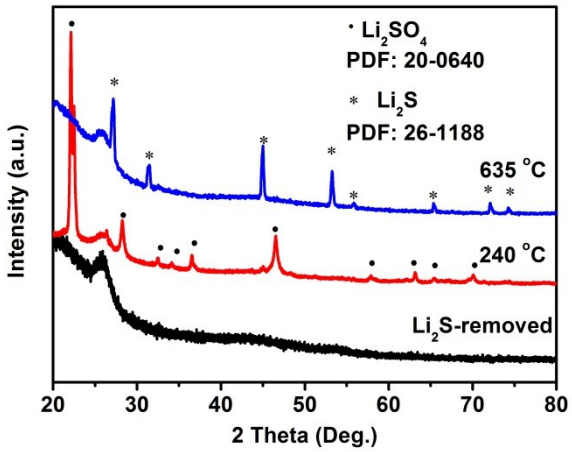

Figure S6. XRD patterns of the samples taken after partial carbonization at 240 °C and after the carbothermal conversion at 635 °C, and of the Li_2S removed C-CNT matrix.

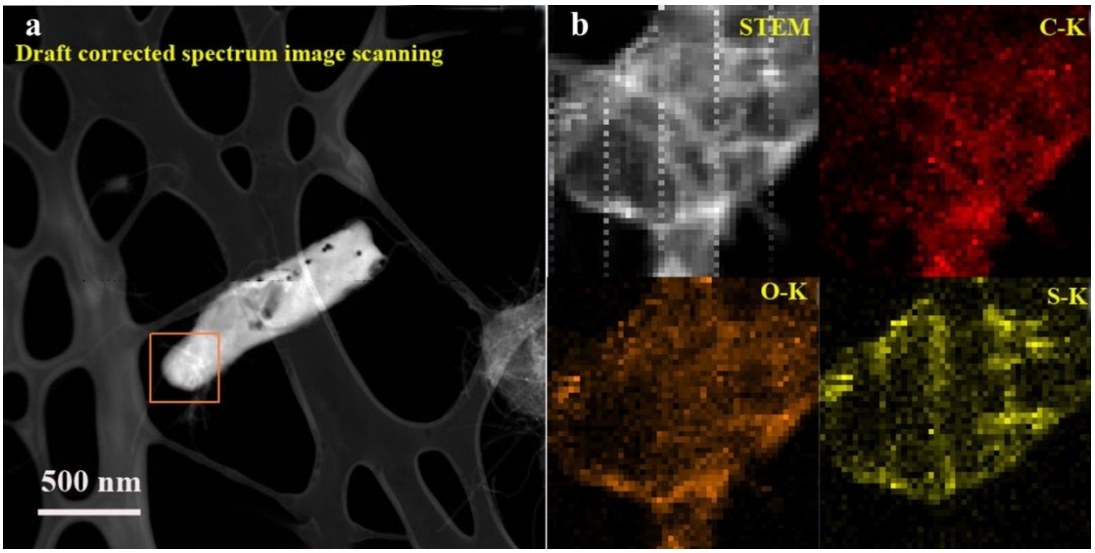

Figure S7. TEM image for the heat-treated Li_2SO_4@PVA nanocomposites at 240 °C (a) and the Elementary mapping of C, S and O (b).

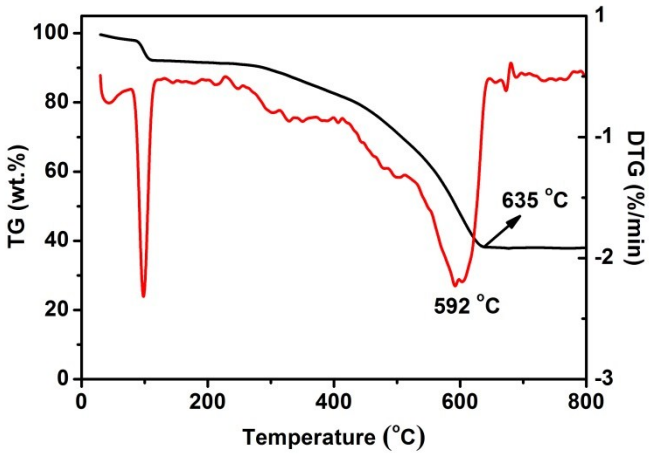

Figure S8. TGA curve in N_2 environment for the heat-treated Li_2SO_4@PVA-CNT nanocomposites electrode at 240 °C.

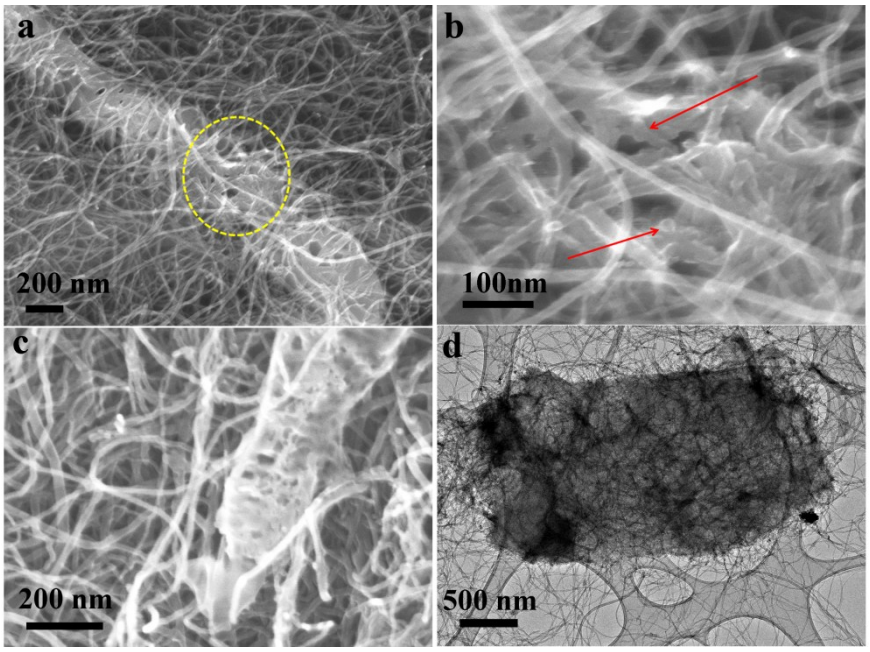

Figure S9. (a) SEM and (b) a high magnification SEM images for Li_2S@C-CNT electrode. (c) SEM and (d) TEM image for Li_2S removed C-CNT matrix by the Li_2S@C-CNT nanocomposite electrode dissolving into ethanol and water.

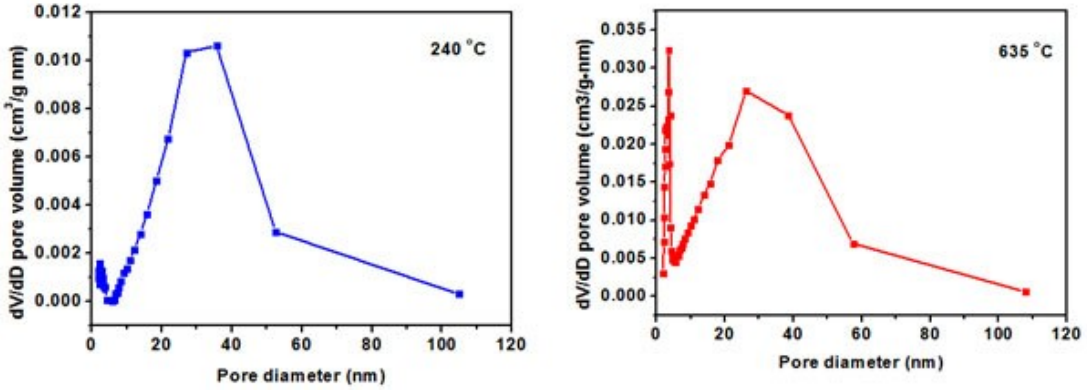

Figure S10. The distribution of pore size for carbon matrix before (240 °C) and after (635 °C) Li_2S formed.

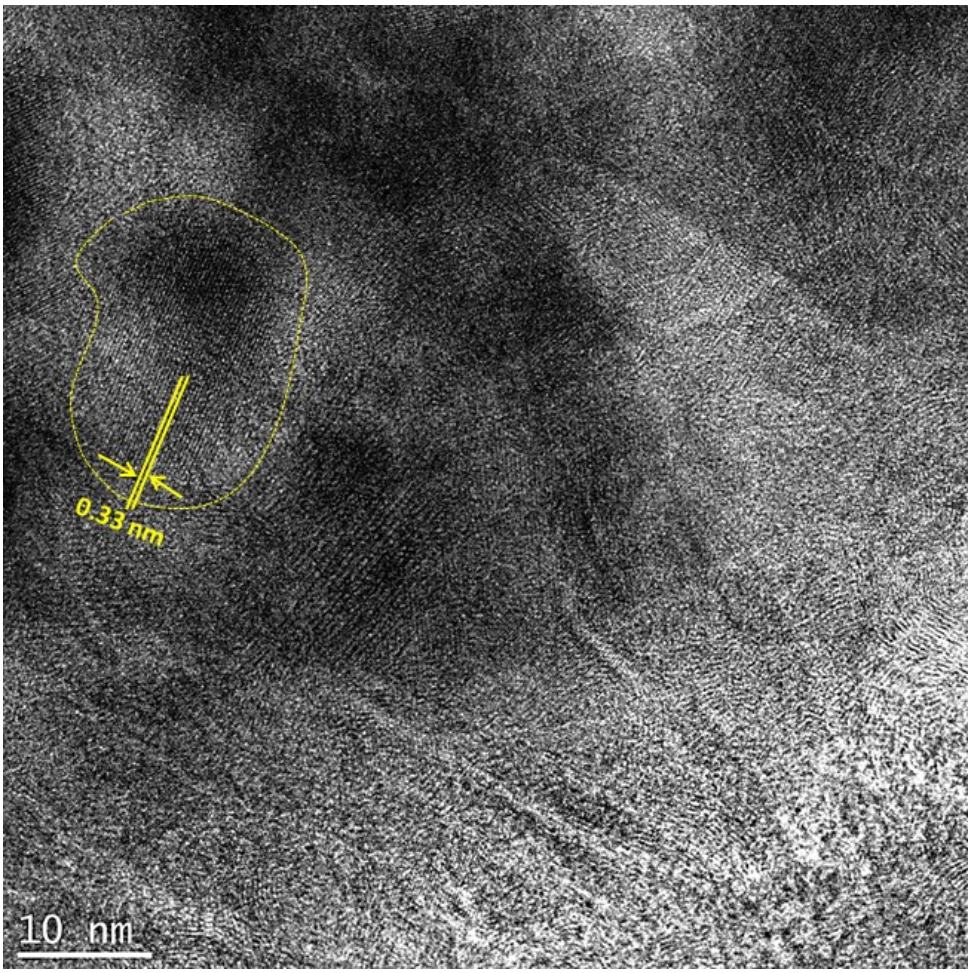

Figure S11. A HRTEM image for the Li_2S@C composite prepared at 635°C. Li_2S particle size and Li_2S crystalline lattice spacing can be identified.

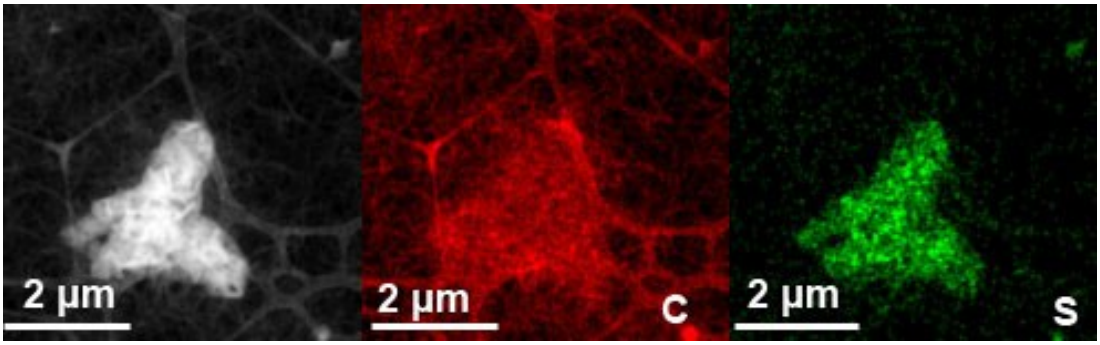

Figure S12. STEM image (left) for the final Li_2S@C nanocomposite strips at 635 °C and the Elementary mapping of C (middle) and S (right).

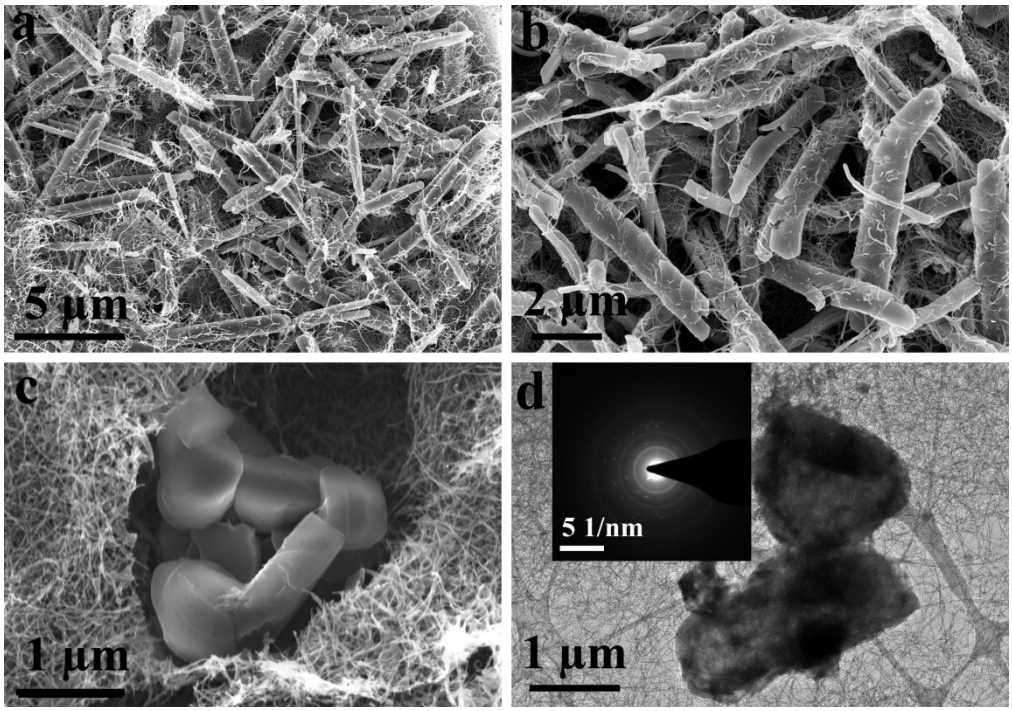

Figure S13. SEM image for (a) as prepared Li_2SO_4-CNT, (b) heat-treated at 240 ^oC, (c) heat-treated at 700 ^oC, and (d) TEM image for Li_2S-CNT electrode heated at 700 ^oC and a SAED image (inset) .

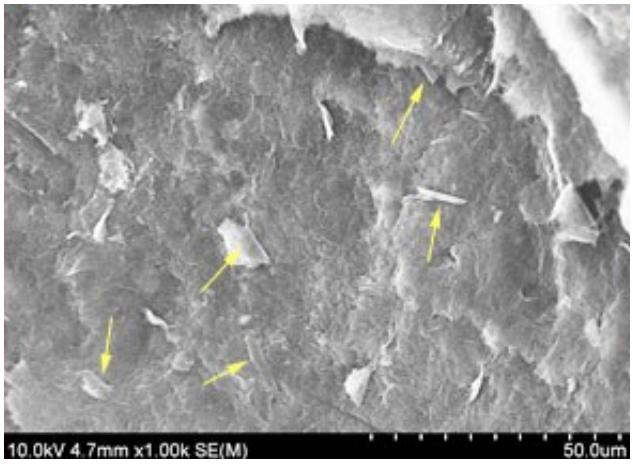

Figure S14. SEM image for Li_2S@C-CNT electrode over 220 cycles at a rate of 1 C.

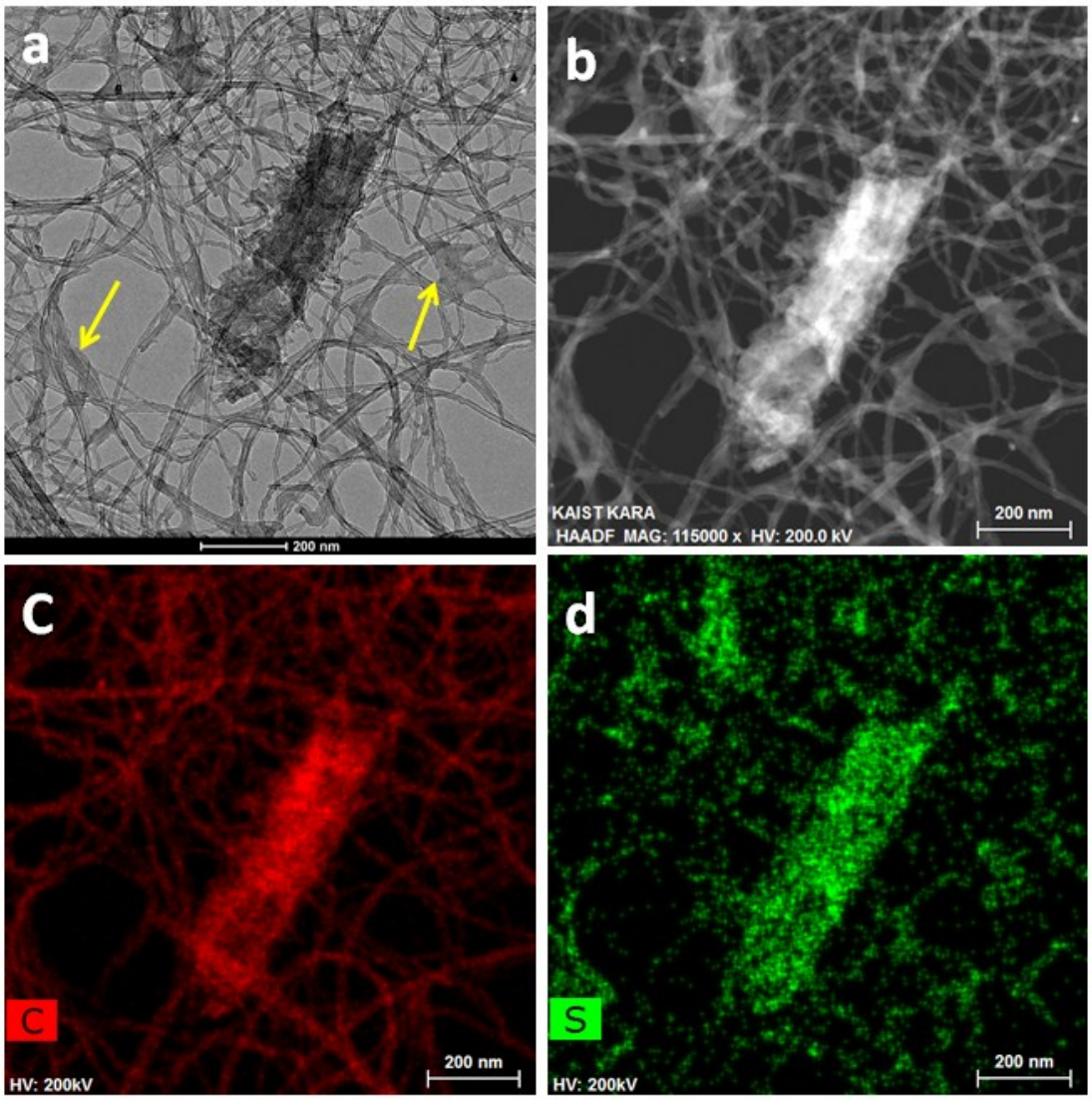

Figure S15. TEM (a) and STEM image (b) for the final Li_2S@ C –CNT after 220 cycles at 1 C and the elementary mapping of C (c) and S (d).

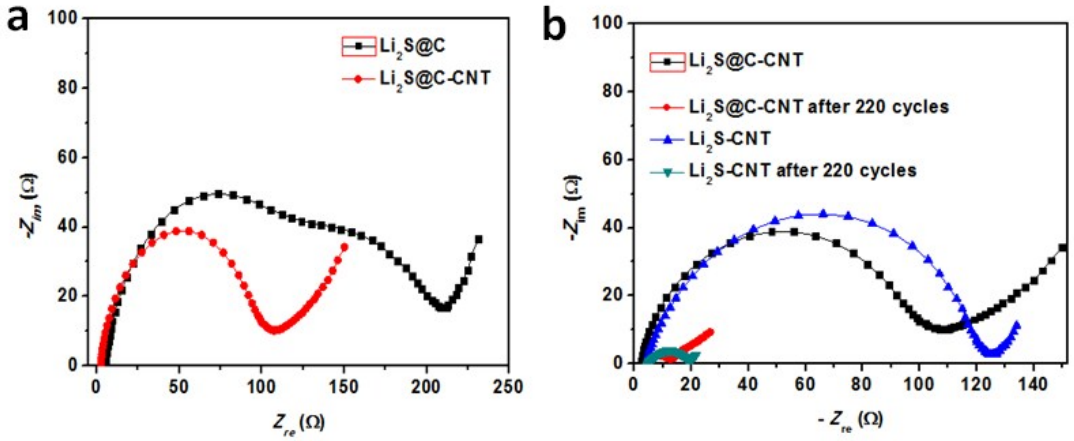

Figure S16. EIS spectrum (a) collected by using Li_2S@C and Li_2S@C-CNT electrode, respectively and (b) The comparison on EIS spectrum before and after cycling for Li_2S-CNT and Li_2S@C-CNT electrodes.

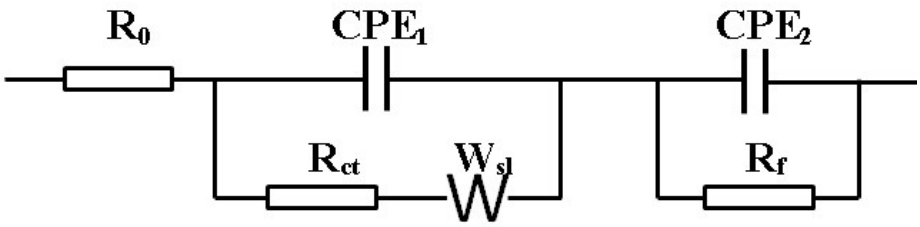

Figure S17. Equivalent circuit for fitting the electrochemical impedance spectra. In this equivalent circuit, R_0 is the ohmic resistance of cells, including electrolyte resistance, R_{ct} is the charge transfer resistance of interface between electrode/electrolyte. R_f is the resistance induced by solid electrolyte interface (SEI) on Li metal anode, CPE_1 and CPE_2 are the constant phase element, W_{sl} means the Warburg impedance controlled by the semi-infinite diffusion.

Table S2. The impedance fitting results for the various electrodes.

	R_o/ Ω	R_{ct}/ Ω	R_f/Ω
Li_2S@C	4.76	131	148
Li_2S@C-CNT	2.51	95.0	88.0
Li_2S-CNT	4.31	118	101
Li_2S@C-CNT (After 220 cycles)	4.31	8.80	6.50
Li_2S-CNT (After 220 cycles)	4.73	15.1	10.6

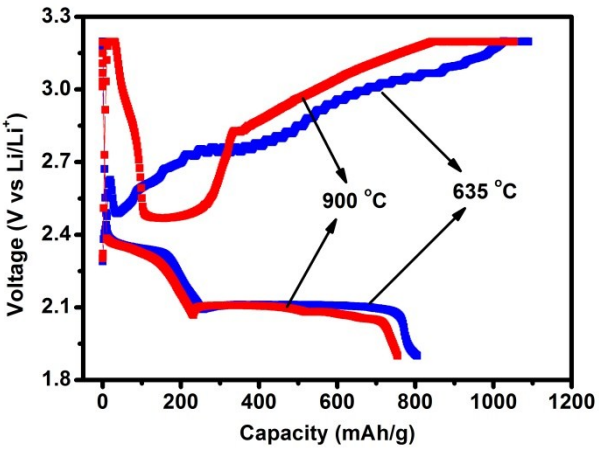

Figure S18. Initial charge-discharge curves for the Li_2S@C-CNT nanocomposite electrodes from two different carbothermal reaction temperatures (635 and 900 °C), respectively.

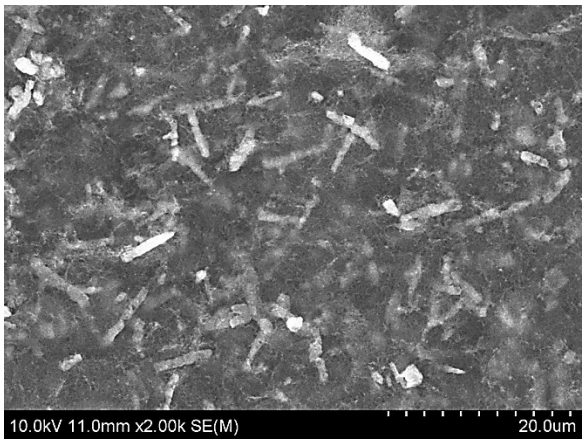

Figure S19. SEM image for Li_2S@C-CNT electrode obtained at 900 ^oC in N_2.

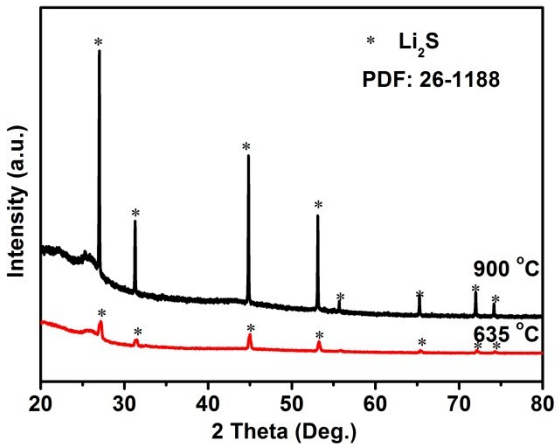

Figure S20. XRD patterns of the Li_2S@C-CNT nanocomposite electrodes from two different carbothermal reaction temperatures of 635 and 900 ^oC, respectively.

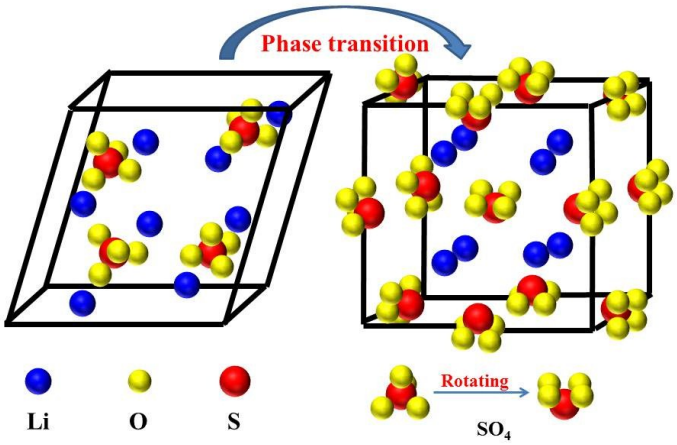

Figure S21. Crystal structure change for Li_2SO_4 at 579 °C.

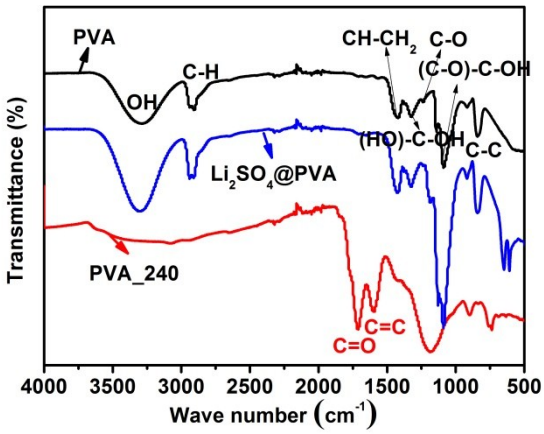

Figure S22. FT-IR spectrum for the pristine PVA, Li_2SO_4@PVA nanocomposites and PVA_240.

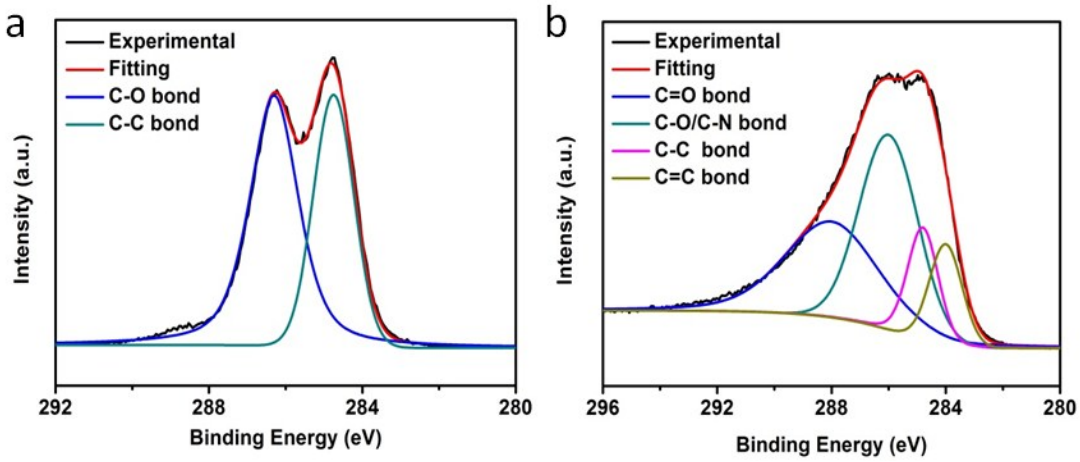

Figure S23. (a) C 1s XPS spectra for the pristine PVA and (b) C 1s XPS Spectra for the partial carbonized PAN in the air at 240 ^{o}C.

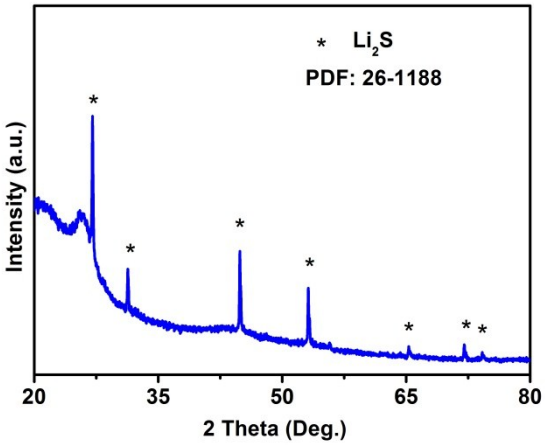

Figure S24. XRD pattern for Li_2SO_4@PAN composite after a heat treatment under N_2 at 635 ^{o}C.

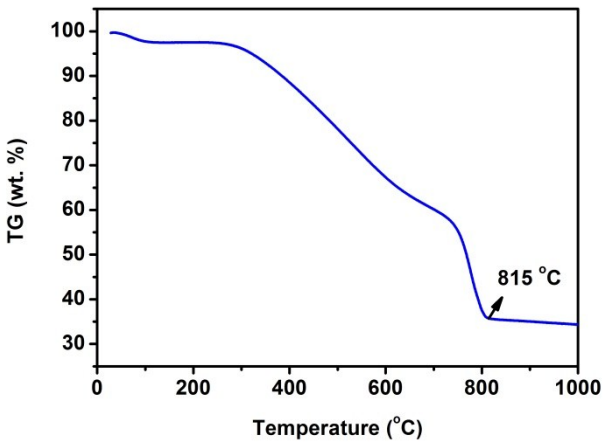

Figure S25. TGA curve in N_2 for the heat-treated Li_2SO_4@RF nanocomposites in the air at 240 °C.

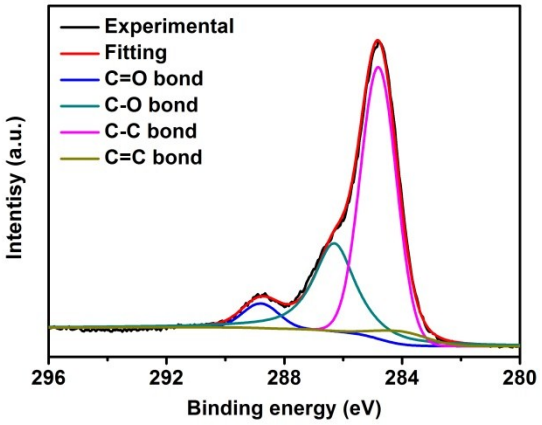

Figure 26. C 1s XPS Spectra for the Li_2SO_4@RF nanocomposites after a heat treatment in the air at 240 °C.

References

[1] Z. Yang, J. Guo, S. K. Das, Y. Yu, Z. Zhou and H. D. Abruna, L. A. Archer, *J. Mater. Chem. A* 2013, **1**, 1433-1440.

[2] M. Kohl, J. Bruckner, I. Bauer, H. Althues and S. *J* Kaskel, *Mater. Chem. A* 2015, **3**, 16307-16312.

[3] J. Liu, H. Nara, T. Yokoshima, T. Momma and T. Osaka, *Electrochim. Acta* 2015, **183**, 70-77.

[4] D. H. Wang, X. H. Xia, D. Xie, X. Q. Niu, X. Ge, C. D. Gu, X. L. Wang and J. P. Tu, *J. Power Sources* 2015, **299**, 293-300.

[5] Z. Li, S. Zhang, C. Zhang, K. Ueno, T. Yasuda, R. Tatara, K. Dokko and M. Watanabe, *Nanoscale* 2015, **7**, 14385-14392.

[6] D. H. Wang, D. Xie, T. Yang, Y. Zhong, X. L. Wang, X. H. Xia, C. D. Gu and J. P. Tu, *J. Power Sources* 2016, **331**, 475-480.